Synthesis and Characterization of Network Single Ion Conductors Based on Comb-Branched Polyepoxide Ethers and Lithium Bis(allylmalonato)borate

Xiao-Guang Sun[†] and John B. Kerr*

Lawrence Berkeley National Laboratory, MS 62-203, One Cyclotron Road, Berkeley, California 94720

Received April 12, 2005; Revised Manuscript Received October 14, 2005

ABSTRACT: Network single ion conductors (NSICs) based on comb-branch polyepoxide ethers and lithium bis(allylmalonato) borate have been synthesized and thoroughly characterized by means of ionic conductivity measurements, electrochemical impedance, and cycling in symmetrical Li/Li half cells, Li/V_6O_{13} full cells in which a NSIC was used as both binder and electrolyte in the cathode electrode and as the electrolyte separator membrane, and by dynamic mechanical analysis (DMA). The substitution of the trimethylene oxide (TMO) unit into the side chains in place of ethylene oxide (EO) units increased the polymer−ion mobility (lower glass transition temperature). However, the ionic conductivity was nearly one and half orders of magnitude lower than the corresponding pure EO-based single ion conductor at the same salt concentration, which may be ascribed to the lower dielectric constant of the TMO side chains that result in a lower concentration of free conducting lithium cations. For a highly cross-linked system (EO/Li = 20), only 47 wt % plasticizing solvent (ethylene carbonate (EC)/ethyl methyl carbonate (EMC), 1/1 by wt) could be taken up, and the ionic conductivity was only increased by 1 order of magnitude over the dry polyelectrolyte, while for a less densely cross-linked system (EO/Li = 80), up to 75 wt % plasticizer could be taken up and the ionic conductivity was increased by nearly 2 orders of magnitude. A Li/Li symmetric cell that was cycled at 85 °C at a current density of 25μA cm^{-2} showed no concentration polarization or diffusional relaxation, which was consistent with a lithium ion transference number of 1. However, both the bulk and interfacial impedance increased after 20 cycles, which was apparently due to continued cross-linking reactions within the membrane and on the surface of the lithium electrodes. A Li/V_6O_{13} full cell constructed using a single ion conductor gel (propylene carbonate (PC)/EMC, 1/1 in wt) was cycled at 25 °C at a current density of 25μA cm^{-2} and showed an initial capacity of 268 mAh g^{-1} of V_6O_{13}, which stabilized at around 200 mAh g^{-1} after the first 20 cycles. During the DMA measurements on the NSICs, it was found that besides the main glass transition (α transition) there was a distinct secondary glass transition (β transition) for NSICs having five EO units in the side chains, while this (the secondary transition) was not clearly visible in the network single ion conductors (NSICs) with shorter side chains (two, three, and four EO units). The main glass transition (α transition) was attributed to the whole network structure of the single ion conductors and secondary glass transition (β transition) appeared to be due to the complexation of lithium by the side-chain chains. Both the main glass transition and the secondary transition were found to shift to higher temperature with increasing salt concentration.

1. Introduction

Solid polymeric electrolytes (SPEs) serve as both the electrolyte and the separator in rechargeable lithium batteries, and they can offer many advantages over commercial liquid electrolytes such as low cost design, flexibility in sizes and shapes, and most importantly in safety, which make them strong candidates for aerospace and electric vehicle batteries. To fulfill the requirements for practical applications, the polymer electrolytes first of all must have adequate transport properties for the dissolved salts at ambient temperature (e.g., the ionic conductivities). Since the ionic conductivity is governed by the number of charge carriers and their mobility, there are two main ways to increase ionic conductivities, i.e., enhancing ionic mobility and maximizing the number of conducting charge carriers. Since the ionic mobility is related to the segmental motion of the polymer, increasing ion mobility can be realized by designing new polymers with lower glass transition temperatures. As a result, comb-shaped polymers with different structures, such as polyphosphazenes,[1−3] polysiloxanes,[4−6] polyvinyl benzyl ethers,[7] and polyepoxide ether,[8−10] have been developed and high ambient temperature ionic conductivities in the range of 10^{-6}−10^{-5} S cm^{-1} have been reported. To increase the number of conducting charge carriers most efforts have been focused on the synthesis of new lithium salts with large anions whose negative charges can be well delocalized to minimize ion pairing with the lithium cation and thus provide more free lithium ions for conduction. Among the new lithium salts, the most favored have been perfluorinated ones such as lithium bis(trifluoromethylsulfonyl)imide (LiTFSI),[11−13] lithium bis(perfluoroethylsulfonyl) imide (LiBETI),[14,15] and lithium tris-(trifluoromethylsulfonyl) methide (lithium methide),[16,17] which have been extensively studied in both liquid and polymer electrolytes during the last 10 years. An alternative approach to increase both ion mobility and the number of charge carriers in polymer electrolytes systems is to add high dielectric constant solvents to yield plasticized polymer electrolytes (or gel polymer electrolytes) and the ionic conductivities of these systems can easily reach 10^{-3} S cm^{-1} at ambient temperature.[18−20]

Despite the progress that has been made in the field of polymer electrolytes for lithium batteries, nearly all of the electrolytes have been binary salt conductors, which suffer from

* To whom correspondence should be addressed. E-mail: jbkerr@lbl.gov. Phone: 1-510-486-6279. Fax: 1-510-486-4995.

[†] Present address: Department of Chemistry and Biochemistry, Arizona State University, Tempe, AZ 85287-1604.

10.1021/ma0507701 CCC: $33.50
Published on Web 11/23/2005

salt concentration changes across the membrane and within the composite electrodes upon the application of continuous, direct current during discharge.[21] This phenomenon is due to the fact that there is no electrode reaction for the anions, which tend to accumulate at the anode unless the salt diffusion coefficient is sufficiently large to allow the concentration gradient to relax. The generation of salt concentration gradients results in voltage losses due to concentration polarization as well as to changes in the transport properties that may result in poorer performance and even undesirable changes in the electrolyte state such as phase transitions or salt precipitation. To avoid concentration polarization, the free movement of anions needs to be limited or totally eliminated. The former case is realized by incorporation of electronically deficient moieties into the polymer chain, which can act as an anion-trapping site to limit the free movement of anions.[22,23] The latter case is realized by covalent attachment of the anions to the polymer backbones[24−45] to form single ion conductors with a unity lithium transference number ($t^0_+ = 1$). The second case has been shown by theoretical modeling to be preferred for practical applications.[46]

In our lab, we have focused on the synthesis of new single ion conductors that could provide sufficiently high mechanical strength to act as a separator and at the same time provide higher ionic conductivity at ambient temperatures.[47−49] This was realized by the synthesis of a new lithium salt, lithium bis(allylmalonato)borate (LiBAMB), which has two allyl groups attached to the anion center. After grafting this salt onto polyacrylate[47] and polymethacrylate ethers[47,48] containing allyl groups through the use of 1,1,3,3-tetramethyldisiloxane in the presence of a Pt catalyst, NSICs were obtained. These materials possessed good mechanical strength, and symmetric Li/Li half-cell cycling showed no evidence of concentration polarization as expected for true single ion conductors. Unfortunately the conductivity was too low due to the unexpectedly poor dissociation of the LiBAMB ion pair, which reduced the concentration of charge carriers and the high glass transition temperature of the polyacrylate and polymethacrylate backbones, which reduced the mobility of the polymer chains and hence the mobility of the solvated lithium ions. In a previous communication we demonstrated that the ionic conductivity of the network type single ion conductors could be improved by use of a more flexible polyepoxide backbone.[49] In this article, we report on these NSICs more thoroughly. We first extend our scope to include trimethylene oxide (TMO) containing segments in these NSICs, as it has been shown in our lab that for the same salt concentration the TMO-containing polyepoxide ethers have lower glass transition temperatures than those of the corresponding pure ethylene oxide (EO) based polyepoxide ethers.[8] Higher mobility of ions and thus higher ionic conductivity is expected. We will also show the initial results of using these NSICs in a full cell, where lithium foil was used as the anode and V_6O_{13} as the cathode in which the single ion conductor was used as the binder as well as the electrolyte in the composite electrode. To the best of our knowledge, this is the first report where a lithium single ion conductor has been used both as the electrolyte membrane and the binder/electrolyte in the composite electrodes. Since the mechanical properties of the polyelectrolyte material are important not only for use in the separator but also in the composite electrode structures, we will also present some results of viscoelastic measurements of these polyepoxide ether based NSICs. These measurements have revealed the existence of two distinct glass transition temperatures for some materials.

2. Experimental Section

2.1. Materials. Allyloxy ethanol, 2-[2-chloroethoxy] ethanol, 3-chloro-1-propanol, 3,4-dihydro-2H-pyran, allyglycidyl ether, tetrabutylamonium hydrogen sulfate, triethylene glycol monomethyl ether, hydrochloric acid, diethyl malonate, trimethyl borate, allyl bromide, trichloromethylsilane, 1,2-dichloroethane, 1,1,3,3-tetramethyldisiloxane, sodium metal, lithium ribbon, toluene, benzene, anhydrous methanol, anhydrous ethanol, Brij 35, anhydrous $MgSO_4$, and NaOH and KOH pellets were all obtained from Sigma-Aldrich and were used directly without further purification. Tetrahydrafuran (Burdick & Jackson, distilled in glass) was refluxed over CaH_2 for several days before use. Platinum−divinyltetramethyldisiloxane complex in vinylsilicon was obtained from Gelest, Inc. V_6O_{13} was a gift from Kerr-McGee Corporation. Carbon for electronic contact in the composite electrodes was Shawinigan Black (Chevron).

2.2. Synthesis. The syntheses of pentaethylene glycol monomethyl ether (Scheme 1) and the intermediate I (Scheme 2), lithium bis{2-[3-(1,1,3,3-tetramethyldisiloxanyl)propyl]malonato} borate, were described previously.[48] The synthesis of TMO-containing monomers was detailed in a previous publication.[8] The synthesis of epoxide monomers and prepolymers followed the literature procedures[8−10,50] and the following are examples of the syntheses that provide sufficient detail to allow synthesis of all of the materials described in this paper. Modification of the procedures to yield different length monomers is achieved by selecting the appropriate starting materials.

2.2.1. Synthesis of Monomers (Scheme 1). 2-(2-Chloroethoxy)-tetrahydropyran was synthesized by the dropwise addition of one molar equiv of 2-chloroethanol to 3,4-dihydro-2H-pyran with concentrated hydrochloric acid as catalyst (1−2 mL per mol of 2-chloroethanol). The crude addition product was dissolved in ether and neutralized with dilute NaOH aqueous solution, washed with distilled water, and dried with anhydrous $MgSO_4$. The solution was filtered and concentrated on a rotary evaporator. The crude product was then distilled, 99% pure by gas chromatography (GC) analysis. ^{1}H NMR ($CDCl_3$, ppm): 4.59 (m, 1H), 3.7−4.0 (m, 2H), 3.3−3.7 (m, 4H), 1.2−1.9(m, 6H).

2-[2-(2-Allyloxyethoxy)ethoxy]tetrahydropyran 2-allyoxyethanol (350 g, 3.43 mol), 2-(2-chloroethoxy)tetrahydropyran (329 g, 2 mol), and tetrabutylammonium hydrogen sulfate (75 g, 0.22 mol) were mixed with 50% aqueous sodium hydroxide solution (640 mL) and toluene (500 mL). The mixture was heated to 70 °C with vigorous mechanical stirring for 16 h. After cooling to room temperature, the mixture was poured into crushed ice (200 g) and mixed well. The upper organic layer was isolated, and the aqueous layer was extracted with ether (100 mL × 3). The organic layers were then combined and washed with H_2O (75 mL × 2) and dried over $MgSO_4$. The solution was concentrated on a rotary evaporator. The volatiles were removed under a vacuum of 0.2 Torr in an oil bath at 130 °C. The residual brownish oil (293 g) in the pot was the crude product. Yield: 64%, 89.6% pure by GC analysis. This crude product was used directly for the next synthesis step.

2-(2-Allyloxy-ethoxy)-ethanol. Crude product of 2-[2-(2-allyloxyethoxy)ethoxy] tetrahydropyran (293 g) was dissolved in ethanol (500 mL), and concentrated HCl (20 mL) in distilled water (50 mL) was added. The solution was refluxed overnight, neutralized with $NaHCO_3$, and concentrated under reduced pressure. The residual oil was vacuum distilled, and the fraction at 77−79 °C/1.2 Torr was collected to obtain the product, 150 g, yield: 81.5%, 98% pure by GC analysis. ^{1}H NMR ($CDCl_3$, ppm): 5.88 (m, 1H), 5.26 (d, 1H), 5.17 (d, 1H), 4.01 (d, 2H), 3.5−3.8 (m, 8H), 2.52 (s, 1H).

2-(2-{2-[2-(2-Methoxyethoxy)ethoxy]ethoxy}ethoxy)tetrahydropyran. Following the same procedure as for 2-[2-(2-allyloxyethoxy)ethoxy]tetrahydropyran, triethylene glycol monomethyl ether (260 g, 1.59mol), *2-(2-Chloroethoxy)tetrahydropyran* (200 g, 1.22 mol), and tetrabutylammonium hydrogen sulfate (56 g, 0.165 mol), 50% sodium hydroxide aqueous solution (490 mL), and toluene (350 mL) were used. After the same work up procedure, a viscous liquid (230 g) was obtained, yield 65%, 84% pure by GC analysis. This crude product was used directly for the next synthesis step.

Scheme 1. Synthesis of Monomers and Prepolymers (Degree of Polymerization Is Indicated by the *Y* Values in the Table and the Proportion of Side Chain to Cross Linker by the *X* Value)[a]

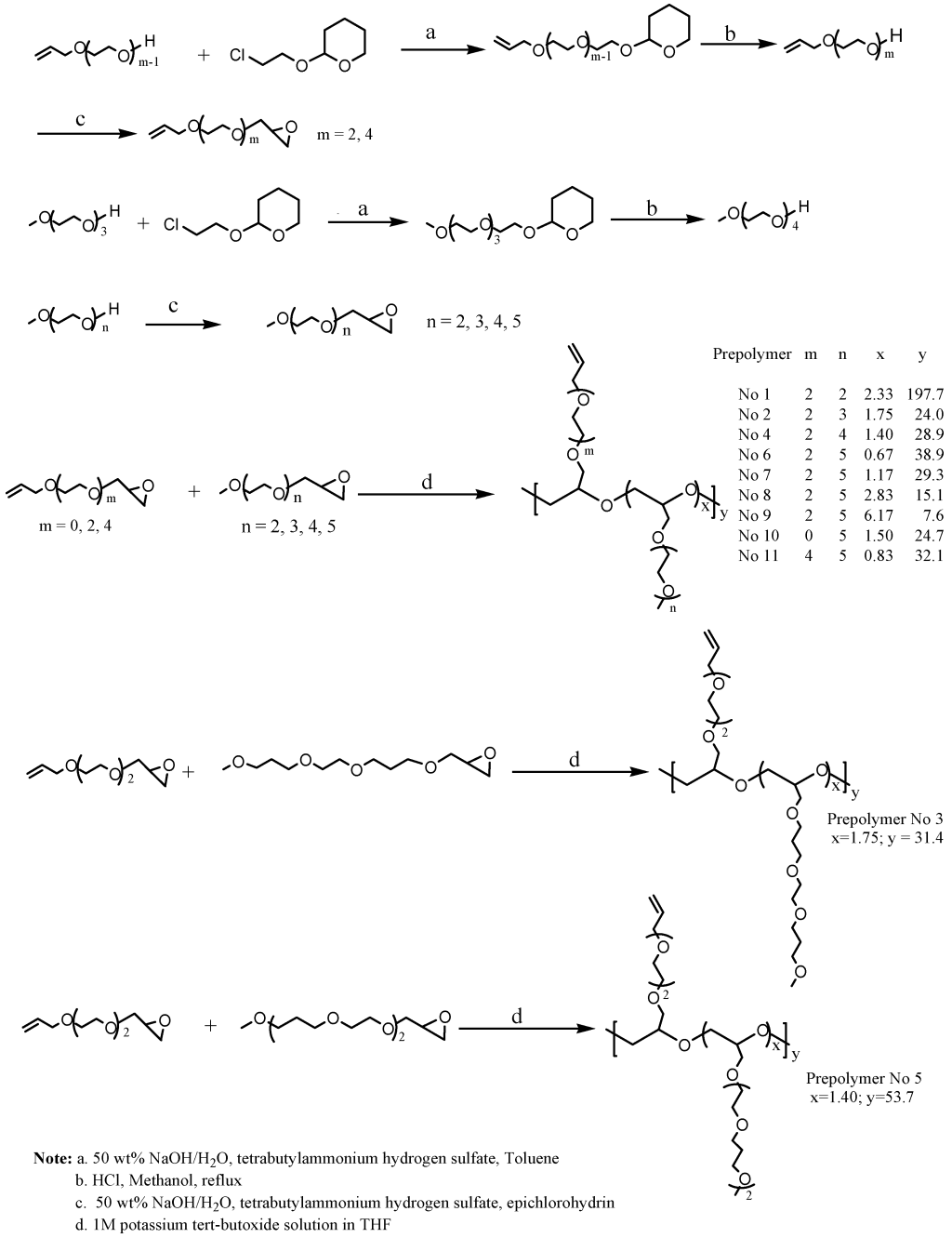

[a] Key: (a) 50 wt% NaOH/H_2O, tetrabutylammonium hydrogen sulfate, toluene; (b) HCl, methanol, reflux; (c) 50 wt% NaOH/H_2O, tetrabutylammonium hydrogen sulfate, epichlorohydrin; (d) 1 M potassium *tert*-butoxide solution in THF.

2-{2-[2-(2-Methoxyethoxy)ethoxy]ethoxy}ethanol. Following the same procedure used for 2-(2-allyloxyethoxy)ethanol, 2-(2-{2-[2-(2-methoxyethoxy)ethoxy]ethoxy}ethoxy)tetrahydropyran (230 g) was hydrolyzed. The product was collected at 102−104 °C/0.4 Torr, 128 g, yield 78.0%, 97% pure by GC analysis. ^{1}H NMR ($CDCl_3$, ppm): 3.4−3.8 (m, 16H), 3.35 (s, 3H), 3.05(s, 1H).

2-[2-(2-allyloxyethoxy)ethoxymethyl]oxirane. 2-(2-Allyloxyethoxy)-ethanol (68 g, 0.47 mol) was mixed with tetrabutylammonium hydrogen sulfate (17 g, 0.05 mol) and 50% aqueous sodium hydroxide solution (190 mL). The solution was mechanically stirred and cooled with an ice bath to 0−5 °C, while epichlorohydrin (250 mL) was added slowly through a dropping funnel. After addition was complete, the reaction was continued with mechanical stirring for 14 h, after which the solution was poured onto crushed ice (100 g) and mixed well. The upper organic layer was isolated, and the aqueous layer was extracted with ether (75 mL × 3). The organic layers were then combined and washed with H_2O (50 mL × 2) and dried over $MgSO_4$. The solution was concentrated on a rotary evaporator. The residual oil was distilled twice from CaH_2, and the fraction at 98−100 °C/0.7 Torr was collected, 47.5 g, yield: 50%, 98.5% pure by GC analysis. ^{1}H NMR ($CDCl_3$, ppm): 5.88 (m, 1H), 5.25 (d, 1H), 5.16 (d, 1H), 4.00 (d, 2H), 3.5−3.9 (m, 9H), 3.41(m, 1H), 3.14 (m, 1H), 2.77 (m, 1H), 2.59(m,1H).

2-(2-{2-[2-(2-methoxyethoxy)ethoxy]ethoxy}ethoxymethyl)-oxirane. Following the same procedure for 2-[2-(2-allyloxyethoxy)-ethoxymethyl]oxirane, 2-{2-[2-(2-methoxyethoxy)ethoxy] ethoxy}-ethanol (79 g, 0.38 mol), tetrabutylamonium hydrogen sulfate (13 g, 0.038 mol), 50% aqueous sodium hydroxide solution (130 mL), and epichlorohydrin (200 mL) were used. The crude product was twice distilled from CaH_2, and the fraction at 136−142 °C/0.1 Torr

Scheme 2. Synthesis of NSICs

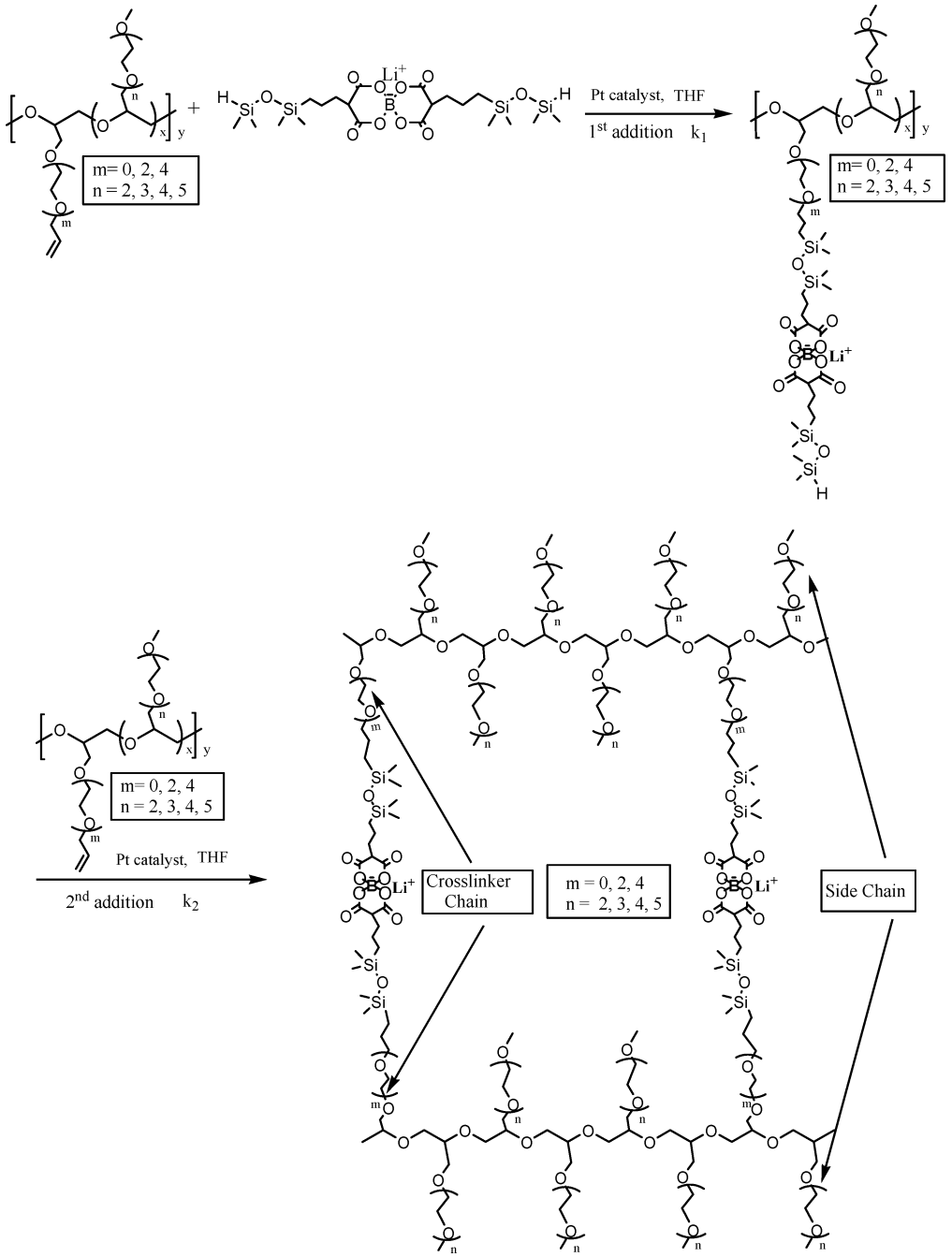

was collected, 60 g, yield: 59%, 98.0% pure by GC analysis. ^{1}H NMR ($CDCl_3$, ppm): 3.5−3.9 (m, 17H), 3.2−3.5 (m, 4H), 3.13 (m, 1H), 2.77 (m, 1H), 2.58 (m, 1H).

2.2.2. Synthesis of Prepolymers (Scheme 1). The synthesis of prepolymers followed the literature procedure[8−10,50] except that the polymerization was initiated under vacuum. The following is a typical example of the synthesis.

Prepolymer No. 4 (see Table 1). To a well-dried 50-mL round-bottom flask was charged 2-[2-(2-allyloxyethoxy)ethoxymethyl]-oxirane (5.5 g, 27.2 mmol) and 2-(2-{2-[2-(2-methoxyethoxy) ethoxy]ethoxy}ethoxymethyl)oxirane (10 g, 37.9 mmol) inside a Helium-filled drybox. A magnetic stirrer was added, and the flask was sealed with a septum. The flask was taken out of the drybox, and it was degassed first and then flushed with dry Argon. The above process was repeated three times, and finally the solution was degassed and heated to 60 °C. Potassium *tert*-butoxide (0.65 mL 1 M) solution in THF was injected into the reaction flask through a syringe. The reaction was continued with stirring at 60 °C for 2 days before it was terminated with methanol (1 mL). The cooled solution was dissolved in dichloromethane (50 mL) and was extracted with deionized water (10 mL). The lower organic layer was separated, and the solvent was removed on a rotary evaporator. The product was further purified by precipitation twice from ether solution into a large amount of hexane. The collected prepolymer was dried under high vacuum over P_2O_5 for 2 days. A light-yellow viscous liquid was obtained, 14.0 g, yield, 90%. Mn 1.12×10^4 g/mol, PDI = 1.47. ^{1}H NMR ($CDCl_3$, ppm): 5.88 (m, 1H), 5.25 (d, 1H), 5.15 (d, 1H), 3.99 (d, 2H), 3.4−3.8 (m, 42.4H), 3.35 (s, 4.2H).

2.2.3. Synthesis of NSICs (Scheme 2). The synthesis of a NSIC is little different from the procedure described in the previous publication.[48] To ensure the complete reaction by the direct film casting technique more catalyst was used than previously reported. Amounts of prepolymers and lithium bis{2-[3-(1,1,3,3-tetramethyldisiloxanyl)propyl]malonato}borate (intermediate I) were mixed in dry THF such that the number of allyl groups in the

Table 1. Physical Properties of Prepolymers and Single Ion Conductors

	prepolymers							single ion conductors		
no.	monomer (I)	cross linker (II)	I/II	$M_n \times 10^4$	Mw $\times 10^4$	PDI	T_g/°C	EO/Li	T_g/°C	Log σ_{25}/S cm^{-1}
1	$EP(EO)_2$	$AllylE_2Ep$	2.33	3.35	12.1	3.61	−75.3	20:1	−47.2	−7.56
2	$EP(EO)_3$	$AllylE_2Ep$	1.75	0.93	1.41	1.52	−74.9	20:1	−53.0	−6.90
3	EP(TMOEOTMO)	$AllylE_2Ep$	1.75	1.11	2.00	1.80	−79.2	20:1	−62.5	−7.40
4	$EP(EO)_4$	$allylE_2Ep$	1.40	1.12	1.65	1.47	−75.2	20:1	−55.3	−6.35
5	$EP(TMOEO)_2$	$allylE_2Ep$	1.40	1.64	3.28	2.00	−80.0	20:1	−61.8	−7.27
6	$EP(EO)_5$	$allylE_2Ep$	0.67	1.16	1.59	1.36	−75.2	10:1	−39.4	−7.51
7	$EP(EO)_5$	$allylE_2Ep$	1.17	1.20	1.65	1.38	−74.4	20:1	−53.1	−6.14
8	$EP(EO)_5$	$allylE_2Ep$	2.83	1.17	1.62	1.38	−74.2	40:1	−65.3	−5.99
9	$EP(EO)_5$	$allylE_2Ep$	6.17	1.11	1.60	1.45	−74.1	80:1	−68.4	−6.23
10	$EP(EO)_5$	AGE	1.50	1.03	1.42	1.38	−73.9	20:1	−57.1	−6.14
11	$EP(EO)_5$	$allylE_4EP$	0.83	1.26	1.75	1.39	−75.2	20:1	−52.7	−6.48

prepolymer was equal to that of Si−H in intermediate I. Pt catalyst (0.5 mol % relative to the double bonds present in the polymer) was added, and the mixture was stirred for 10 min. The homogeneous solution was then cast in glass rings on the surface of a Teflon plate inside a drybox dedicated for use with organic solvent vapors. The solvent was allowed to evaporate slowly. The formed films were then heated to around 60 °C for 48 h to ensure the reaction was as complete as possible. Transparent self-standing films with thicknesses varying from 50 to 150 μm were obtained. These films were further dried in the antechamber of the drybox in the presence of P_2O_5 for 2 days.

2.3. Measurements. ^{1}H and ^{13}C NMR (TMS as internal reference) spectra were collected on a Bruker 300 NMR Spectrometer. GC measurements were performed on a 5890 Series II plus Gas Chromatograph with a Supelco SPB5 fused silica column (30 m, 0.32 mm inside diameter, film thickness 0.25 μm) and carrier gas of Helium (3 mL/min) with a temperature program of 5 min at 40 °C, 10 °C/min to 230 °C and 5 min at 230 °C. The molecular weights of the prepolymers were determined by use of an Agilent 1100 series HPLC equipped with a refractive index detector. A PLgel 10-μm miniMIX-B 250 × 4.6 mm column (Polymer Laboratories, Ltd) was employed with THF eluent (0.3 mL/min) and calibrated by using polystyrene standard samples (Polymer Laboratories, EasyCal) in THF with molecular weights ranging from 500 to 3 000 000.

Glass transition temperatures (T_g) were measured using a Perkin-Elmer-7 differential scanning calorimetry (DSC) instrument. The heating rate was 10 °C/min. Viscoelastic measurements were performed on a Rheometric Solid Analyzer (RSAII) in compression mode at a frequency of 1 Hz to measure the temperature dependence of the storage moduli (E'), loss moduli (E''), and loss factor tan δ of the films. The viscoelastic spectra were recorded from −85 to 100 °C at a heating rate of 2 °C /min.

The measurement of alternating current (AC) conductivity was carried out using Swagelok cells that have been described before.[47] A Solartron SI 1254 four-channel frequency response analyzer and a 1286 electrochemical interface were used to measure the impedance of the electrolyte films of known thickness in constant volume cells with blocking electrodes. Li/Li cells were constructed and sealed inside a helium filled drybox, and the cell cycling was carried out at 85 °C using an Arbin BT 4020 multichannel cycler. The cell cycling sequence was 1 h relaxation, 2 h charge, 1 h relaxation, and 2 h discharge.

Post-mortem analysis of the polymer membranes was performed by scraping the electrolytes off the electrode and the total weight of the electrolyte was weighed and dissolved in deionized water (2.0 mL). A standard solution was obtained by dissolving 0.1 g of diethylene glycol monoethyl ether into dichloromethane (100 mL). Such a solution (5 mL) was used to extract the aqueous electrolyte solution. The lower dichloromethane solution was separated through a separation funnel, and 1 mL was taken for analysis by GC.

Gel electrolytes were prepared by addition of dried solvents to the dry membranes prepared as described above. Solvents were dried in the glovebox over molecular sieves or by treatment with superactivated alumina. The amount of plasticizer solvent within the membrane was calculated by the weight difference of the dry membrane before swelling and that of the gel after swelling, which was performed in a helium filled glovebox.

Composite cathode electrodes were prepared by casting a well stirred solution of V_6O_{13} (30 wt % of the final composite electrode), NSIC (58% by total weight of the no. 8 prepolymer in Table 1, intermediate I, and Pt catalyst to provide a final salt concentration of EO/Li = 40), carbon black (10%) and Brij35 (2%) in dry THF on to stainless steel foil. The solvent THF was evaporated inside the solvent drybox, and the resulting electrode was heated at 60 °C overnight and then dried continuously under vacuum in the presence of P_2O_5 in the glovebox antechamber for 2 days. The dried cathode electrode was then cut into disks and used to construct coin cells in which lithium metal foil was used as anode. The membrane used in the full cell was a dry single ion conductor (no. 9 in Table 1) that was saturated in PC/EMC (1/1, wt/wt) solution. The cell was charged and discharged at a current density of 25 μA cm^{-2} with a voltage range of 3.25−2.0 V. During the charge step the current was maintained at 25 μA cm^{-2} until the voltage reached 3.22 V, after which the cell voltage was maintained at 3.25 V until the current density was lower than 2 μA cm^{-2}. The cell was left to relax for 2 h before the next step of discharge. During discharge step under the current density of 25 μA cm^{-2} the cell was switched off when the voltage reaches 2.0 V. The cell was then allowed to relax for 2 h before the next charge step was begun.

3. Results and Discussions

3.1. Synthesis of Monomers and NSICs. As shown in Scheme 1, the allyl-terminated and methoxy-terminated, dihydropyran-protected oligoethylene glycols were synthesized by phase transfer catalyzed nucleophilic addition of shorter chain segments using tetrabutylammonium hydrogen sulfate (THS) as catalyst, and the resulting product was hydrolyzed under acidic conditions. GC was used to monitor the process, and the identity of the distilled product was confirmed by ^{1}H NMR. The purity of the product was greater than 97% as determined by GC. The epoxide ether monomers were obtained by reaction of the allyl- or methoxy-terminated glycols with epichlorohydrin using the same phase transfer catalyst except that epichlorohydrin was used both as reactant and solvent. High-purity epoxide monomer (>97%) was obtained by distillation of the crude product twice from calcium hydride. It was found in practice that the distillation process was crucial, since the trace water removal not only eliminated the ring-opening product (glycols) in the monomer during the distillation process but also guarded against initiator deactivation during the polymerization process.

The prepolymers were obtained by anionic polymerization using potassium *tert*-butoxide as the initiator at 60 °C. They were purified by repeated precipitations from ether solution into a large amount of hexane. The prepolymers were all viscous liquids with glass transition temperature around −75 °C for pure EO-based ones and −80 °C for TMO-containing ones (see Table 1). The molecular weights were in the range of 10−30k, and

the low molecular weight fractions could be removed by fractionation with THF and hexane.

NSICs were obtained by reaction of the prepolymers with lithium bis{2-[3-(1,1,3,3-tetramethyldisiloxanyl)propyl]malonato} borate in the presence of the platinum−divinyltetramethyldisiloxane catalyst. To ensure as complete a reaction as possible, a higher catalyst concentration, i.e., 0.5% concentration relative to the double-bond concentration in the prepolymer, was used (by comparison 0.2% catalyst concentration was used for polyacrylate ether based NSICs[48]). The network-formation process, like the case of potassium hydroxide catalyzed addition of divinyl sulfone to cellulose,[51] can be visualized to proceed in two steps. The first addition of a double bond of the cross-linker chain to one of the Si−H bonds of the salt attaches the salt fragment to the polymer followed by the second addition of the double bond of another cross-linker side chain to the other Si−H bond of the salt (see Scheme 2). Only the second addition leads to a cross-linked network. It should be noted that the two reaction steps have different rates. The first double-bond addition occurs between a compound of low molecular weight and a side chain of the prepolymer (rate constant k_1). The second addition occurs between two side chains of the prepolymer, while one of them is the grafted salt with one pendant Si−H group (rate constant k_2) and hence $k_1 \gg k_2$. However, it is very likely that the two processes could proceed at the same time when the initial concentration of Si−H was high and this was consistent with the observation that as long as the solvent was evaporated inside the drybox, self-standing films were formed (usually within 2 h). After the initial solidification the rate of the second reaction becomes much slower due to the restricted mobility of the polymer chains. Curing of the films at higher temperature (60 °C) increases the rate constant, k_2, and can drive the network formation forward. However it is still limited by the availability of appropriate reacting sites (double bond or Si−H) nearby, which is promoted by the random thermal movement of the polymer side chains. Therefore, the second step addition may continue to occur whenever the matching reactive sites approach each other. This continued curing apparently occurred in the symmetric Li/Li cells that were cycled at 85 °C under charge/discharge conditions and are described below.

3.2. Ionic Conductivity. It was shown in the previous communication[49] for the polyepoxide ether based NSICs with the same cross-linker side chain at the same salt concentration of EO/Li = 20 that the conductivity systematically increases as the side chain length increases up to five EO units ($n = 4$, Scheme 2). It was also shown that the maximum ionic conductivity was observed at a salt concentration of EO/Li = 40.[49] Figure 1 shows the comparison of the conductivities of NSICs containing TMO units with those of corresponding pure EO-based NSICs at the same salt concentration of EO/Li = 20. It is interesting to note that for both prepolymers and the final NSICs the glass transition temperatures of the TMO-containing materials are much lower than those of corresponding pure EO-based ones (see Table 1). This is consistent with previously observed results of binary salt polymer solutions[8] and indicates greater chain mobility of the TMO-containing polymers and thus high mobility of lithium cation of the corresponding NSIC. However, the ionic conductivities shown in Figure 1 for the TMO-containing single ion conductors (TMOEOTMO and EOTMOEOTMO in the side chains) were at least half an order of magnitude lower than those of pure EO-based single ion conductors (EOEOEO and EOEOEOEO in the side chains). Since there are only two factors controlling

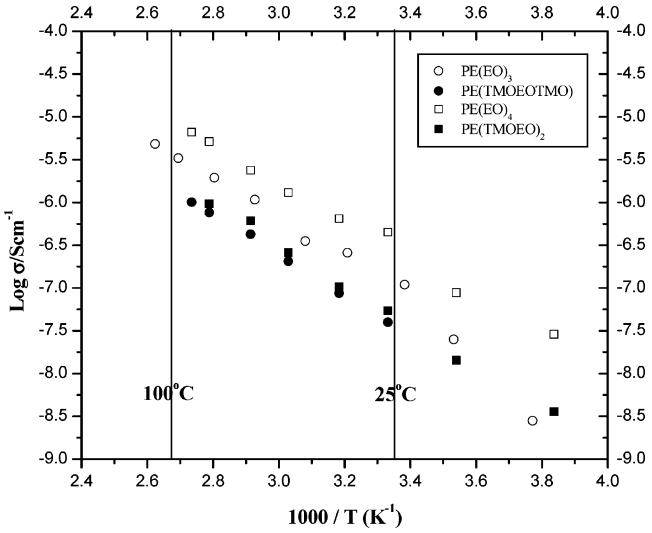

Figure 1. Ionic conductivities of TMO-containing NSICs and those of pure EO-based NSICs at the same salt concentration of EO/Li = 20.

the total ionic conductivity of lithium single ion conductors, i.e., the number of free lithium cations and the cation mobility, these results suggest that the TMO-containing single ion conductors have fewer free conducting lithium cations than those of pure EO-based ones. This is believed to be due to the lower dielectric constant of TMO-containing polymers and steric crowding around the lithium ions that leads to a lower binding energy and hence a decrease in the salt dissociation for the case of the TMO-containing units as compared to the pure EO units.[8b]

Figure 2 shows the ionic conductivities of gel single ion conductors. Figure 2A shows the case of a NSIC with a salt concentration of EO/Li = 20 (no. 7, Table 1) containing different amounts of EC/EMC (1/1), while Figure 2B shows the case of a NSIC with a salt concentration of EO/Li = 80 (no. 9, Table 1) containing 75 wt % of a variety of solvents and solvent mixtures. First of all for both salt concentrations, the ionic conductivities increase with the addition of plasticizer as was also observed for polyacrylate ether based NSICs[47] and comb-shape alkylsulfonate single ion conductors.[52] This is thought to be mainly due to both the increase of ion mobility from the liquid-phase solvation of the lithium ions and the increased concentration of free conducting lithium cations resulting from the high dielectric constant of the solvents[53−56] that favor the dissociation of the salt. However, important differences between the two systems should be noted. The EO/Li = 20 system (Figure 2A) is a highly cross-linked system that can only be swollen by up to 50 wt % of plasticizer solvent, and the ionic conductivity is increased by only 1 order of magnitude. The EO/Li = 80 system (Figure 2B) is a less densely cross-linked system that can be swollen by up to 75 wt % plasticizer, and consequently, the ionic conductivity is increased by nearly 2 orders of magnitude over the dry system. It should also be noted that there is some difference between the polyacrylate ether based gel NSICs and the polyepoxide ether based ones. For polyacrylate ether based single ion conductors, the materials can easily hold 50 wt % plasticizer even for the highly cross-linked system (EO/Li = 10),[47] while the swollen polyepoxide ether based single ion conductor can barely hold 50 wt % plasticizer (only 47 wt %) for a less cross-linked system (EO/Li = 20). This observation may indicate that the polyacrylate ether based single ion conductors were less efficiently cross linked than the corresponding polyepoxide ether based single ion conductors at the same salt concentration. This might be

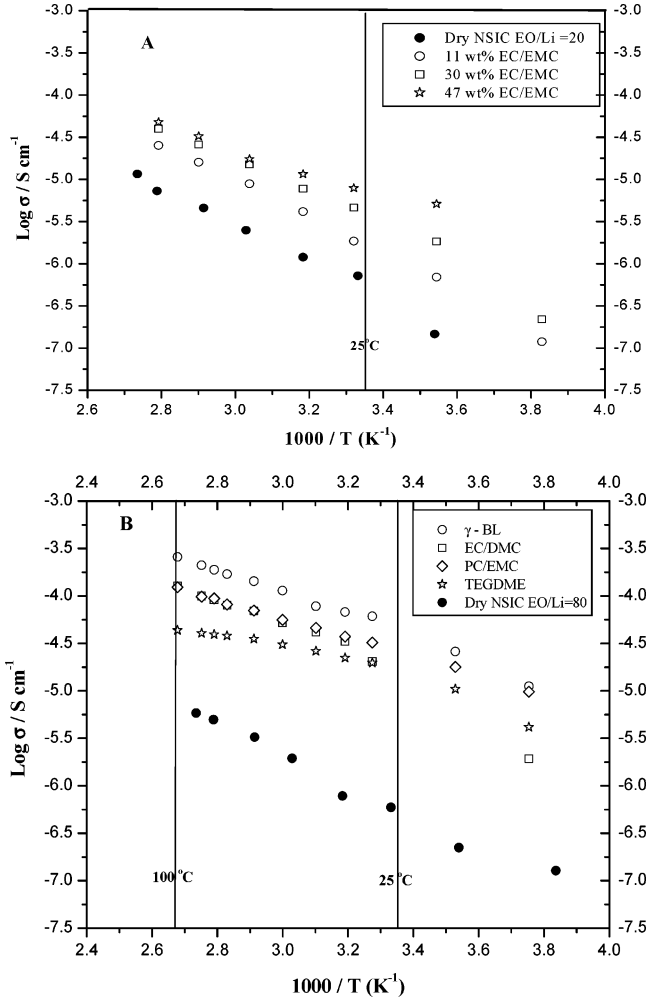

Figure 2. The ionic conductivities of gel single ion conductors. (A) EO/Li = 20 (no. 7, Table 1) with different amounts of EC/EMC. (B) EO/Li = 80 (no. 9, Table 1) with 75 wt % of a variety of solvents.

directly related to the cross-linker side-chain length, i.e., one EO unit was used to connect the allyl group for the polyacrylate ether based single ion conductor while two EO units were used for the polyepoxide ether based single ion conductor. The longer, more flexible cross-linker chain should facilitate a more efficient second step addition (Scheme 2). The lower flexibility of the acrylate backbone may also play a role in the observed difference, and the end result is that, although the first step addition proceeded smoothly for both systems, the second step addition was apparently less efficient for the polyacrylate system.

Figure 3 shows the ionic conductivities of the dry NSICs with different cross-linker chain lengths at the same salt concentration of EO/Li = 20. When the cross-linker chain length increases from 0 EO units (allylglycidyl ether (AGE) monomer) to 2 EO units, the resulting NSIC shows nearly the same ionic conductivity. However, when the cross-linker chain length is increased to 4 EO units, the ionic conductivity does not increase as observed for polyacrylate ether based single ion conductors but decreases instead, which is believed to be related to more efficient cross linking that results in a slightly higher glass transition temperature (Table 1), lower polymer mobility, and thus lower ionic mobility. These effects are relatively small but may be important if they are indeed related to the efficiency of the curing reactions. Further detailed study of the curing reactions is necessary and will be reported on later.

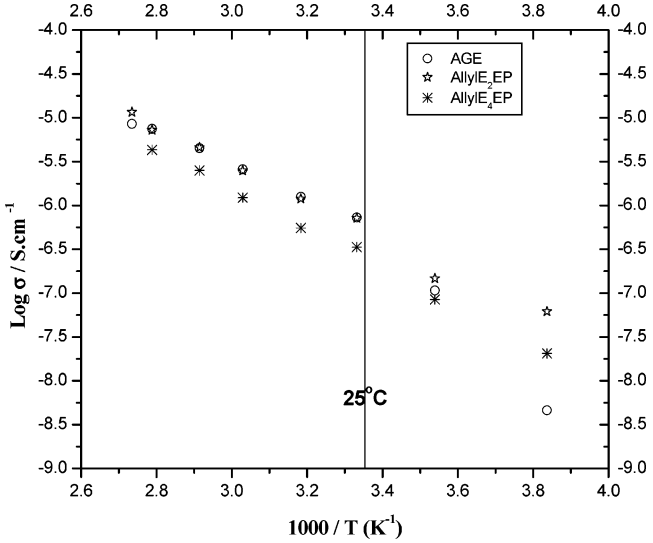

Figure 3. Ionic conductivities of NSICs with different cross linkers at the same salt concentration of EO/Li = 20.

3.3. Cell Cycling. *3.3.1. Li/Li Cell Cycling.* The NSIC sample with the highest conductivity (no. 8, Table 1) was used to construct a symmetrical Li/Li cell with two lithium foil electrodes. The cell was cycled at 85 °C at a current density of 25 μA cm^{-2} with a cycling sequence of 1 h relaxation, 2 h charge, 1 h relaxation, and 2 h discharge. The cycling profile of the cell voltage was shown in a previous communication,[49] and as expected for a true single ion conductor, neither concentration polarization nor diffusion relaxation of the voltage was observed, which was distinctly different from that of a binary salt system in which the cell potential increases over a time period of minutes to hours due to the salt concentration polarization.[8a] The cycling was stopped after 20 cycles, and the cell impedance was measured using AC electrochemical impedance spectroscopy. It was found that both the bulk ($R_{b)}$) and interfacial (R_{int}) impedances increased. The increase of bulk impedance indicates a decrease in the bulk conductivity of the membrane which may be due to continued reaction of unreacted Si−H groups with free allyl groups to form further network cross links that reduce polymer mobility. As mentioned in section 3.1, the second double-bond addition will continue whenever there is a possibility of the two reactive sites coming into contact (the platinum catalyst is not removed from the polymer). This is first facilitated by the higher temperature (85 vs 60 °C for curing), i.e., increased chain mobility, and second facilitated by the charge/discharge conditions where the migration of the lithium ions may increase the segmental motion of the anion back and forth and increase its chance of meeting a nearby double bond. These combined effects result in an increase in the cross-link density of the electrolyte membrane, which lowers the mobility of the polymer chains and thus leads to lower conductivity and higher impedance. The increase of the interfacial impedance suggests a reaction of the single ion conductor with the lithium electrode at the electrode/electrolyte interface, which results in the immobilization of polymer chains at the interface and thus lowers the mobility of the ions passing through the interface and yields a higher interfacial impedance. Such a process is reflected in the cycling profile by an increase in the potential with continued cycling.

The cell cycling was continued after impedance measurement, and it was observed that the cell potential increased very rapidly with cycling and soon exceeded the safety limit. It was also observed at the same time that there were signs of concentration polarization and concentration relaxation with continued cycling.

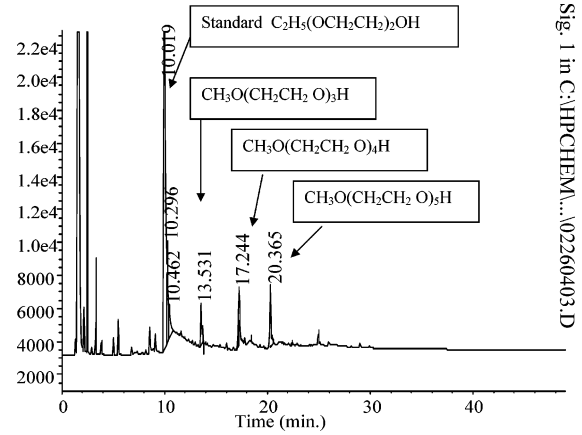

Figure 4. GC trace of the extraction of the failed lithium cell in Figure 4. Dichloromethane is used as solvent and helium as carrier gas.

This suggested that some small, mobile anionic species were produced due to covalent bond cleavage, and this was confirmed from the postmortem GC analysis of the dichloromethane extract of the cycled NSIC sample. As shown in Figure 4, the side-chain fragment, pentaethylene glycol monomethyl ether, and further cleaved smaller fragments, tetraethylene glycol monomethyl ether and triethylene glycol monomethyl ether, were found in the extraction, thereby confirming the occurrence of bond cleavage. Although the GC analysis does not detect anionic species, it seems reasonable that similar bond cleavage will occur on the chains that connect the anions also. Previously with the polyacrylate ether NSICs, such decomposition was measured qualitatively.[48] In this case, the decomposition was measured quantitatively by use of an internal standard, and the result showed that the decomposed product was approximately 1.3 wt % of the total amount of the NSIC in the separator membrane. This represents a significant degree of reaction at the lithium electrode, particularly as the GC method does not detect any charged ionic species that may also be released. The very large interfacial impedance appears to be linked to this degradation. Even at such low current densities of 25 μA cm^{-2}, the impedance is sufficiently large to cause bond cleavage while forcing the current through the interface. This may indicate that the chain segments in the NSIC are very restricted in motion next to the electrode surface and consequently resist the passage of the ions. This evidence for bond cleavage suggests an alternative cause for the rise in interfacial impedance that results from depletion of anion concentration next to the electrode. The appearance of some small amount of concentration polarization appears to confirm that anionic groups are released.

3.3.2. Li/V_6O_{13} Cell Cycling. Figure 5 shows the discharge profiles of the full cell, Li/NSIC gel (PC/EMC)/V_6O_{13}, at different cycle numbers. The membrane is a gel single ion conductor with a salt concentration of EO/Li = 80, which was obtained by saturation of the corresponding dry single ion conductor (no. 9, Table 1) with a PC/EMC (1/1, wt/wt) mixture. The cell was cycled at ambient temperatures (25 ± 10 °C) at a current density of 25 μA cm^{-2}. As described in the Experimental Section, the cathode electrode was made from a NSIC with a salt concentration of EO/Li = 40 (no. 8, Table 1). This is the first report in the literature we are aware of where a full cell was built by using a single ion conductor both as the membrane and the electrode binder. The discharge curve shows the typical three-step profile of V_6O_{13} cathode material with an initial discharge capacity of 268 mAh g^{-1}. The discharge capacity falls to around 200 mAh g^{-1} in the following cycle and then slowly increases to 225 mAh g^{-1} until the tenth cycle and thereafter

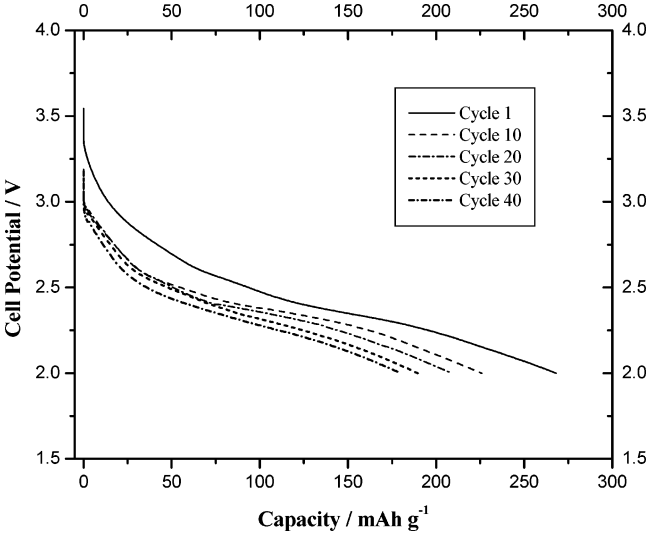

Figure 5. The discharge profiles of the full cell Li/V_6O_{13} under the current density of 25 μA cm^{-2} at different cycles at 25 °C. The membrane was a fully saturated (with PC/EMC, 1/1 by weight) dry single ion conductor with a salt concentration of EO/Li = 80, membrane area = 1 cm^2, and active material V_6O_{13} = 1.68 mg.

slowly decreases again. The observed initial capacity trend appears to be related to the fact that initially there is no solvent in the cathode electrode where the NSIC weight constitutes 58% of the electrode weight. The solvent in the membrane diffuses together with the lithium ions into the composite cathode electrode during the discharge, which results in an increase of ionic conductivity in the composite cathode electrode and leads to more utilization of active material (V_6O_{13}) and consequently to the observed gradual increase in the discharge capacity within the first 10 cycles. It seems that at the tenth cycle this process reaches the equilibrium and the following decrease in capacity is mainly due to the gradual loss of activity of the active material. The fluctuations in capacity appear to be related to temperature variations as the cell was not thermostated.

A full investigation of the electrochemical behavior of the NSIC materials in composite electrodes is beyond the scope of this report. Suffice to say that the elimination of salt concentration gradients at and within the electrodes has been shown to provide some of the benefits expected from the modeling of the behavior of single ion conductors in composite electrodes.[46] The maintenance of the cell capacity demonstrated in Figure 5 is in contrast to the capacity fading observed for V_6O_{13} at 85 °C with binary salt electrolytes.[57] The loss of capacity in the binary salt cells is at least partly caused by salt concentration gradients that generate concentration polarization and alter the exchange current densities at the electrodes and hence the interfacial impedances. Slow relaxation of the salt gradients leads to loss of usable capacity in the cell on continued cycling. It should pointed out that the very large interfacial impedances observed with NSIC electrolytes are a major impediment to their practical use as useful rates are unattainable. There appear to be significant differences between the behaviors of the NSICs at the electrode surfaces compared to the bulk of the membrane which is consistent with the rheological literature on the behavior of polymers at surfaces.[58] To begin to understand the behavior of these NSIC materials it is important to report on their mechanical properties and an initial study on the bulk properties is reported below.

3.4. Viscoelastic Properties. Figure 6 shows the dynamic mechanical analysis of the NSICs in which the storage modulus (E'), loss modulus (E''), and loss tangent (tan δ) were measured

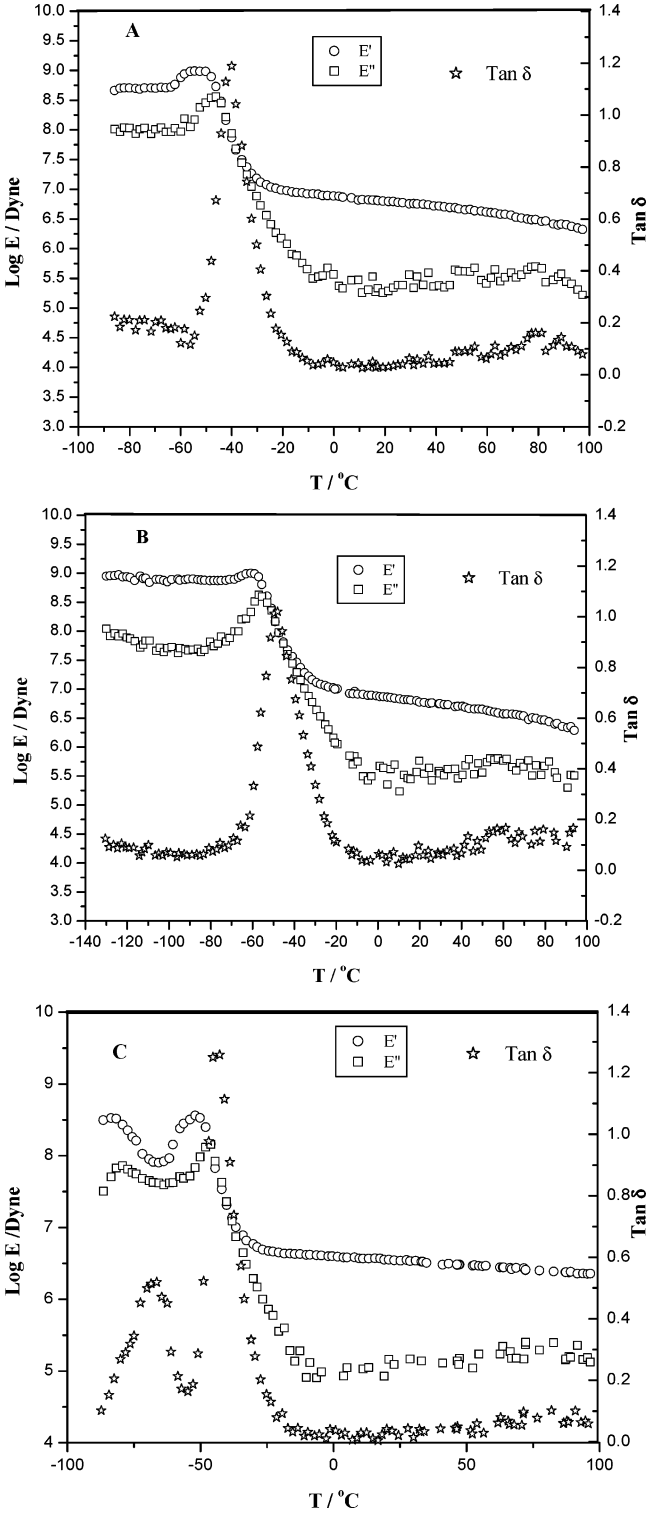

Figure 6. Storage modulus (E'), loss modulus (E''), and loss tangent (tan δ) data were measured as a function of temperature at 1 Hz. (A) $PEPE_3$-based NSIC (no. 2 in Table 1); (B) PE(TMOEOTMO)-based NSIC (no. 3 in Table 1); (C) $PEPE_5$-based NSIC (no. 7 in Table 1).

at 1 Hz and plotted as a function of temperature. Figure 6A shows the data of a $PEPE_3$-based NSIC (no. 2 in Table 1, $n = 3$, $m = 2$ in Scheme 2), Figure 6B shows that of PE(TMOEOTMO)-based NSIC (no. 3 in Table 1), while Figure 6C shows that of $PEPE_5$-based NSIC (no. 7 in Table 1, $n = 5$, $m = 2$ in Scheme 2). These three systems were chosen to illustrate the effect of structure on the mechanical behavior, i.e., the comparison between parts A and B of Figure 6 reflects differences between pure EO side chains and TMO-containing side chains, and the comparison between parts A and C of Figure 6 reflects the effect of side chain length. The loss modulus (E'') and loss tangent (tan δ) in parts A and B of Figure 6 both show a major transition peak at lower temperatures, which is attributed to the main glass transition temperature (α transition) of the network structure of the single ion conductors. It is noted in these two figures that the glass transition temperature of TMO-containing single ion conductor is lower than that of the pure EO-based single ion conductor, which is consistent with the T_g values measured by DSC (temperatures measured by dynamic mechanical analysis are 10−12 °C higher due to differences in calibration). In both parts A and B of Figure 6, additional broad peaks are barely visible in the tan δ plot in the temperature range of 50−100 °C. These peaks may be due to the "ionic clusters" as observed in comb-shape sulfonate ionomers[59,60] or carboxylate ionomers.[61,62] It should be noted, however, that in the ionomers reported in the literature the anions were only fixed to one polymer side chain so the anions had more opportunity to aggregate at temperatures higher than the glass transition or melting temperatures. The opportunity for "ionic cluster" formation in the NSICs where the anions are fixed between two polymer side chains is likely to be more constrained except for the less than perfectly formed network as mentioned above, which leaves some one-end free anions as in the case of comb-shape ionomers. However, the percentage of these one-end free anions is small so it is consistent that they result in barely visible peaks as compared to the relatively large peaks in the comb-shape ionomers.

A small peak in the tan δ at high temperature is also barely visible in Figure 6C for the $PEPE_5$-based single ion conductor at a salt concentration of EO/Li = 20. The distinct difference between part C of Figure 6 and parts A and B of Figure 6 is the additional transition peak observed at the low-temperature range of −100 to −50 °C. This is a secondary glass transition (or β transition) relative to the main transition and may originate from the complexation of lithium cations by the oligoether side chains. The difference between part C of Figure 6 and parts A and B of Figure 6 suggest that the 5 EO units in the side chain is long enough to form a distinguishing domain that can be detected by the dynamic mechanical analysis, as the secondary transition was not distinctly observed for the $PEPE_2$-, $PEPE_3$-, and $PEPE_4$-based single ion conductors. The secondary glass transition due to the complexation of lithium by the oligoether side chains was also reported in the literature for an amorphous comblike polymer based on methylvinyl ether/maleic anhydride alternating copolymer backbone with oligooxyethylene side chains,[63] though the two transition temperatures were well separated due to the large difference in mobility between the backbone and side chains. Similar secondary transitions are also observed in other $PEPE_5$-based single ion conductors with different salt concentrations as shown in Figure 7 in which for clarity only the low temperature range is displayed. It is interesting to note, however, both the main glass transition and secondary transition shift to higher temperature with increasing salt concentration. The shift in the main glass transition is mainly due to the increased cross-linking density of the network as salt concentration is increased. The shift in secondary transition is primarily due to more complexation of lithium cations by the side chains.[63] Another observation in Figure 7 is that the peak height of the β transition decreases relative to the main glass transition at high salt concentration, indicating that the material becomes less mobile as a whole due to the higher cross-linking density. The β transition relative peak height of the lowest concentration is also lower than the intermediate concentration,

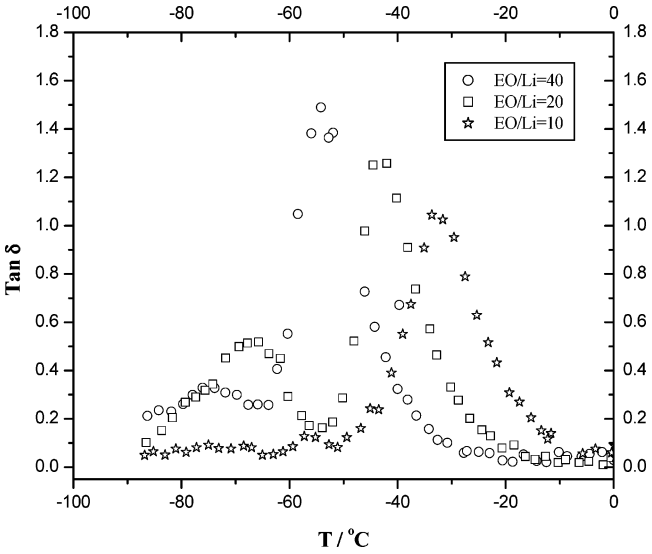

Figure 7. Loss tangent (tan δ) data was measured as a function of temperature at 1 Hz for $PEEO_5$-based NSICs at different salt concentrations (nos. 6−8 in Table 1).

and this may indicate a smaller effect due to the lower concentration of lithium. Further studies are necessary to elucidate these points.

Conclusions

The lower ionic conductivities of the NSICs containing TMO compared to the corresponding pure EO-based single ion conductors suggest that for an increase in ionic conductivity (for both binary salt polymer electrolytes and single ion conductors) it is necessary to balance between increasing ion mobility by increasing flexibility with the TMO groups and decreasing the charge carrier number; otherwise the gain in polymer mobility may not compensate for the loss in the number of free conducting lithium cations. The behavior of the malonatoborate anion used in this study appears to be quite sensitive to changes in the dielectric constant of the medium and the small change induced by the introduction of the extra methylenes in the TMO-containing side chains appears to cause a large increase in the ion pairing of the anion and the lithium cations. More polarizable anions such as bis(trifluoroalkylsulfonyl)imide ($(CF_3SO_2)N^-$) appear to be less affected by this change judging from the behavior of the binary salts in TMO-containing polyepoxide ethers.[8] The synthesis of appropriately structured polyelectrolytes with this anion is in process to further test this hypothesis.

The postmortem analysis of the cycled Li/Li symmetric cells suggests that the polyepoxide ethers are not stable to metallic lithium and may require the use of carbon anodes as used in lithium ion batteries. However, binary salt systems of similar polymer structure do not show such instability. The instability is probably related to the large interfacial impedances observed at the lithium and composite electrodes which are orders of magnitude higher than those observed with binary salt polymer electrolytes.[57,64] Such large impedances prevent the use of the cells at practical rates (hence the use of 25 μA cm^{-2} for both Li/Li and Li/V_6O_{13} cell cycling) and the source of the impedance may be attributed partly to the inhibition of the polymer motion at the electrode surface of the NSIC. There also appears to be a fundamental effect upon the kinetics of the electrode reaction that results in low exchange current densities and large interfacial impedances. The nature of the surface interactions and the resulting morphology is likely to be critical for a solution to this problem. The viscoelastic measurements of the bulk NSIC materials demonstrate that there are two transitions (α and β transition) for 5 EO-based units NSICs while there is only an α transition for shorter side chain (two, three and four EO units) based materials. The two transitions (α and β transition) are attributed to the backbone (network) and side-chain motion, respectively, and both are affected by salt concentration. This also implies that the side-chain motion can still occur when the network is immobile, which could be very important for maintaining ion mobility at the electrode surfaces. The mechanical measurements also hint at the possibility of ion cluster formation and the development of interesting morphological possiblities with the synthesis of new single ion conductors where the anion is not attached to the cross links but is to a freely moving side chain. Work is proceeding on polymer structures to investigate these possibilities.

Acknowledgment. Special thanks to Mr. Yongbong Han for his assistance in gel single ion conductivity measurement and full cell Li/V_6O_{13} assembly and Dr. Gao Liu for providing TMO-containing monomers. The authors are grateful for the financial support from NASA PERS program (NASA Glenn).

References and Notes

(1) Blonsky, P. M.; Shriver, D. F.; Austin, P.; Allcock, H. R. *J. Am. Chem. Soc.* **1984**, *106*, 6854.
(2) Allcock, H. R.; Prange, R.; Hartle, T. J. *Macromolecules* **2001**, *34*, 5463.
(3) Allcock, H. R.; O'Connor, S. J. M.; Olmeijer, D. L.; Napierala, M. E.; Camer, C. G. *Macromolecules* **1996**, *29*, 7544.
(4) Liang, W. J.; Kao, H. M.; Kuo, P. L. *Macromol. Chem. Phys* **2004**, *205*, 600.
(5) Zhang, Z.; Sherlock, D.; West, R.; West, R.; Amine, K.; Lyons, L. J. *Macromolecules* **2003**, *36*, 9176.
(6) Siska, D. P.; Shriver, D. F. *Chem. Mater.* **2001**, *13*, 4698.
(7) Pantaloni, S.; Passerini, S.; Croce, F.; Scrosati, B.; Roggero, A.; Andrei, M. *Electrochim. Acta* **1989**, *34*, 635.
(8) (a). Kerr, J. B.; Sloop, S. E.; Liu, G.; Han, Y. B.; Hou, J.; Wang, S. *J. Power Sources* **2002**, *110*, 389. (b). Kerr, J. B.; Liu, G.; Curtiss, L. A.; Redfern, P. C. *Electrochim. Acta* **2003**, *48*, 2305.
(9) Marchese, L.; Andrei, M.; Roggero, A.; Passerini, S.; Prosperi, P.; Scrosati, B. *Electrochim. Acta* **1992**, *37*, 1559.
(10) Buriez, O.; Han Y. B.; Hou, J.; Kerr, J. B.; Qiao, J.; Sloop, S. E.; Tian, M.; Wang, S. *J. Power Sources* **2000**, *89*, 149.
(11) Tominaga, Y.; Ohno, H. *Chem. Lett.* **1998**, *9*, 955.
(12) Alloin, F.; Sanchez, J. Y.; Armand, M. B. *Electrochim. Acta* **1992**, *37*, 1729.
(13) Roux, C.; Sanchez, J.-Y. *Solid State Ionics* **1994**, *72*, 160.
(14) Naoi, K.; Mori, M.; Naruoka, Y.; Lamanna, W. M.; Atanasoski, R, *J. Electrochem. Soc.* **1999**, *146*, 462.
(15) Appetecchi, G. B.; Henderson, W.; Villano, P.; Berrettoni, M.; Passerini, S. *J. Electrochem. Soc.* **2001**, *148*, A1171.
(16) Ghigo, G.; Tonachini, G.; Fossey, J. *J. Phys. Org. Chem.* **1997**, *10*, 885.
(17) Dominey, L. A.; Koch, V. R.; Blakley, T. J. *Electrochim. Acta* **1992**, *37*, 1551.
(18) Allcock, H. R.; Kellam, E. C., III; Morford, V. M. *Solid State Ionics* **2001**, *143*, 297.
(19) (a). Sun, X. G.; Lin, Y.; Ding, L.; Jing, X. *Electrochim. Acta* **1996**, *41*, 1573. (b). Sun, X. G.; Lin, Y.; Jing, X. *Eur. Polym. J* **1996**, *32*, 801. (c). Sun, X. G.; Li, B.; Lin, Y.; Jing, X. *Polym. Int.* **1996**, *41*, 301.
(20) Chung, S. H.; Heitjans, P.; Winter, R.; Bzaucha, W.; Florjanczyk, Z.; Onoda, Y. *Solid State Ionics* **1998**, *112*, 153.
(21) Thomas, K. E.; Sloop, S. E.; Kerr, J. B.; Newman, J. *J. Power Sources* **2000**, *89*, 132.
(22) (a) Mehta, M. A.; Fujinami, T.; Inoue, T. *J. Power Sources* **1999**, *81*−*82*, 724. (b) Mehta, M. A.; Fujinami, T.; Inoue, S.; Matushita, K.; Inoue, T. *Electrochim. Acta* **1999**, *45*, 1175.
(23) (a) Sun, X. G.; Angell, C. A. *Electrochim. Acta* **2001,** *46*, 1467. (b) Sun, X. G.; Xu, W.; Zhang, S. S.; Angell, C. A. *J. Phys.: Condens. Matter* **2001**, *13*, 8235. (c) Xu, W.; Sun, X. G.; Angell, C. A. *Electrochim. Acta* **2003**, *48*, 2255.
(24) Bannister, D. J.; Davies, G. R.; Ward, I. M.; McIntyre, J. E. *Polymer* **1984**, *25*, 1291.
(25) Ito, K.; Ohno, H. *Solid State Ionics* **1995**, *79*, 300.

(26) Zhou, G. B.; Khon, I. M.; Smid, J. *Polym. Commun.* **1989**, *30*, 52.
(27) Kobayashi, N.; Uchiyama, M.; Tsuchida, E. *Solid State Ionics* **1985**, *17*, 307.
(28) Zhou, G. B.; Khon, I. M.; Smid, J. *Macromolecules* **1993**, *26*, 2202.
(29) Tsuchida, E.; Ohno, H.; Kobayashi, N.; Ishizaka, H. *Macromolecules* **1989**, *22*, 1771.
(30) Zhang, S. S.; Liu, Q. G.; Yang, L. L. *Polymer* **1994**, *35* (7), 3740.
(31) Benrabah, D.; Sylla, S.; Alloin, F.; Sanchez, J. Y.; Armand, M. *Electrochim. Acta* **1995**, *40* (13 and 14), 2259.
(32) Onishi, K.; Matsumoto, M.; Nakacho, M.; Shigehara, K. *Chem. Mater.* **1996**, *8*, 469.
(33) Fujinami, T.; Tokimune, A.; Mehta, M. A.; Shriver, D. F.; Rawsky, G. C. *Chem. Mater* **1997**, *9*, 2236.
(34) Watanabe, M.; Suzuki, Y.; Nishimoto, A. *Electrochim. Acta* **2000**, *45*, 1187.
(35) Bayoudh, S; Parizel, N.; Reibel, L. *Polym. Int.* **2000**, *49*, 703.
(36) Florjanczyk, Z.; Bzducha, W.; Langwald, N.; Dygas, J. R.; Kork, F.; Misztal-Faraj, B. *Electrochim. Acta* **2000**, *45*, 3563.
(37) Xu, W.; Angell, C. A. *Solid State Ionics* **2002**, *147*, 295.
(38) Snyder, J. F.; Ratner, M. A.; Shriver, D. F. *J. Electrochem. Soc.* **2003**, *150* (8), A1090.
(39) Doyle, M.; Wang, L.;Yang, Z.; Choi, K. *J. Electrochem. Soc.* **2003**, *150* (11), D185.
(40) Sun, X. G.; Angell, C. A. *Solid State Ionics* **2004**, *175* (1−4), 743.
(41) Doeff, M. M.; Reed, J. S. *Solid State Ionics* **1998**, *115*, 109.
(42) Sandi, G.; Carrado, K. A.; Joachin, H.; Lu, W.; Prakash, J. *J. Power Sources* **2003**, *119*, 492.
(43) Singhal, R. G.; Capracotta, M. D.; Martin, J. D.; Khan, S. A.; Fedkiw, P. S. *J. Power Sources* **2004**, *128*, 247.
(44) Walls, H. J.; Riley, M. W.; Fedkiw, P. S.; Spontak, R. J.; Baker, G. L.; Khan, S. A. *Electrochim. Acta* **2003**, *48*, 2071.
(45) Geiculescu, O. E.; Yang, J.; Blau, H.; Bailey-Walsh, R.; Creager, S. E.; Pennington, W. T.; DesMarteau, D. D. *Solid State Ionics* **2002**, *148*, 173.
(46) Doyle, M.; Fuller T. F.; Newman, J. *Electrochim. Acta* **1994**, *39*, 2073.
(47) Sun, X. G.; Liu, G.; Xie, J.; Han, Y.; Kerr, J. B. *Solid State Ionics* **2004**, *175* (1−4), 713.
(48) Sun, X. G.; Reeder, C.; Kerr, J. B. *Macromolecules* **2004**, *37* (6), 2219.
(49) Sun, X. G.; Kerr, J. B.; Reeder, C. L.; Liu, G.; Han, Y. B. *Macromolecules* **2004**, *37* (14), 5133.
(50) Nishimoto, A.; Agehara, K.; Furuya, N.; Watanabe, T.; Watanabe, M. *Macromolecules* **1999**, *32*, 1541.
(51) Lionetto, F.; Sannino, A.; Maffezzoli, A. *Polymer* **2005**, *46*, 1796.
(52) Sun, X. G.; Hou, J.; Kerr, J. B. *Electrochim. Acta* **2005**, *50* (5), 1139.
(53) Saito, Y.; Capiglia, C.; Yamamoto, H.; Mustarelli, P. *J. Electrochem. Soc.* **2000**, *147*, 1645.
(54) Deepa, M.; Sharma, N.; Agnihotry, S. A.; Singh, S.; lal, T.; Chandra, R. *Solid State Ionics* **2002**, *152−153*, 253.
(55) Svanberg, C.; Bergman, R.; Borjesson, L.; Jacobsson, P. *Electrochim. Acta* **2001**, *46*, 1447.
(56) Aihara, Y.; Arai, Shigemasa.; Hayamizu, K. *Electrochim. Acta* **2000**, *45*, 1321.
(57) Kerr, J. B.; Han, Y. B.; Liu, G.; Reeder, C.; Xie, J.; Sun, X. G. *Electrochim. Acta* **2004**, *50*, 234.
(58) Tsagaropoulos, G.; Eisenberg, A. *Macromolecules* **1995**, *28*, 6067.
(59) Agarwal, P. K.; Makowski, H. S.; Lundberg, R. D. *Macromolecules* **1980**, *13*, 1679.
(60) Weiss, R. A.; Fitzgerald, J. J.; Kim, D. *Macromolecules* **1991**, *24*, 1071.
(61) Gauthier, M.; Eisenberg, A. *Macromolecules* **1990**, *23*, 2066.
(62) Kim, J. S.; Wu, G.; Eisenberg, A. *Macromolecules* **1994**, *27*, 814.
(63) Lin, Y.; Qi, L.; Chen, D.; Wang, F. *Solid State Ionics* **1996**, *90*, 307.
(64) Persi, L.; Croce, F.; Scrosati, B.; Plichta, E.; Hendrickson, M. A. *J. Electrochem. Soc.* **2002**, *149* (2), A212.

MA0507701